

Structural basis for recognition of the Sec4 Rab GTPase by its effector, the Lgl/tomosyn homologue, Sro7

Kelly Watson^{a,b}, Guendalina Rossi^a, Brenda Temple^{c,d}, and Patrick Brennwald^{a,b}

^aDepartment of Cell Biology and Physiology, ^bGraduate Program in Cell and Developmental Biology, ^cDepartment of Biochemistry and Biophysics, and ^dR. L. Juliano Structural Bioinformatics Core, University of North Carolina School of Medicine, Chapel Hill, NC 27599

ABSTRACT Members of the tomosyn/Lgl/Sro7 family play important roles in vesicle trafficking and cell polarity in eukaryotic cells. The yeast homologue, Sro7, is believed to act as a downstream effector of the Sec4 Rab GTPase to promote soluble N-ethylmaleimide-sensitive factor adaptor protein receptor (SNARE) assembly during Golgi-to-cell surface vesicle transport. Here we describe the identification of a Sec4 binding site on the surface of Sro7 that is contained within a cleft created by the junction of two adjacent β -propellers that form the core structure of Sro7. Computational docking experiments suggested four models for interaction of GTP-Sec4 with the Sro7 binding cleft. Further mutational and biochemical analyses confirmed that only one of the four docking arrangements is perfectly consistent with our genetic and biochemical interaction data. Close examination of this docking model suggests a structural basis for the high substrate and nucleotide selectivity in effector binding by Sro7. Finally, analysis of the surface variation within the homologous interaction site on tomosyn-1 and Lgl-1 structural models suggests a possible conserved Rab GTPase effector function in tomosyn vertebrate homologues.

Monitoring Editor

Thomas F. J. Martin
University of Wisconsin

Received: Apr 17, 2015

Revised: Jul 9, 2015

Accepted: Jul 14, 2015

INTRODUCTION

Polarized exocytosis requires the proper localized delivery, docking, and fusion of secretory vesicles with sites of active growth on the plasma membrane. In the budding yeast *Saccharomyces cerevisiae*, secretory vesicles are delivered to specific plasma membrane sites where the Rab GTPase Sec4 mediates vesicle tethering through its interaction with the Exocyst complex subunit Sec15 (Walch-Solimena *et al.*, 1997; Guo *et al.*, 1999). After vesicle tethering, a trans-soluble N-ethylmaleimide-sensitive factor adaptor protein receptor (SNARE) complex forms between the vesicle SNARE proteins Snc1/2 and the plasma membrane SNARE proteins Sec9 and Sso1/2, which drives vesicle fusion

(Aalto *et al.*, 1993; Protopopov *et al.*, 1993; Brennwald *et al.*, 1994).

Genetic screens in yeast identified a Sec9-binding protein, Sro7, as an important regulator of Golgi-to-cell surface trafficking (Kagami *et al.*, 1998; Lehman *et al.*, 1999). Sro7 is a member of the structurally conserved Lethal giant larvae (Lgl)/tomosyn family of proteins involved in polarity. Lgl was first discovered in *Drosophila melanogaster*, in which mutant Lgl larvae suffer from imaginal disk outgrowth and show many of the properties of human tumor behavior, such as loss of tissue architecture and cell shape and failure to differentiate (De Lorenzo *et al.*, 1999). The exact mechanism of function for this family of proteins in cell polarity is controversial (Vasioukhin, 2006). Studies on *Drosophila* Lgl suggest that it functions in regulating actin polarity by interacting with myosin II (Strand *et al.*, 1994). Mammalian Lgl is also known to interact antagonistically with the Cdc42-Par6-atypical protein kinase C (aPKC) polarity complex to maintain the identity of the apical and basolateral membranes in epithelial cells (Hutterer *et al.*, 2004). The neuronal family member tomosyn-1 (or Stxbp5) forms a complex with syntaxin-1, SNAP25, and synaptotagmin, directly competing with VAMP (synaptobrevin) for forming an active SNARE complex (Fujita *et al.*, 1998; Ashery *et al.*, 2009). This suggests that tomosyn functions in polarity by regulating neurotransmitter release by affecting the

This article was published online ahead of print in MBoc in Press (<http://www.molbiolcell.org/cgi/doi/10.1091/mbc.E15-04-0228>) on July 22, 2015.

Address correspondence to: Patrick Brennwald (pjbrennw@med.unc.edu).

Abbreviations used: aPKC, atypical protein kinase C; GST, glutathione S-transferase; GTP γ S, guanosine 5'-3-O-(thio)triphosphate; Lgl, Lethal giant larvae; SNARE, soluble N-ethylmaleimide-sensitive factor adaptor protein receptor; t-SNARE, target membrane SNARE.

© 2015 Watson *et al.* This article is distributed by The American Society for Cell Biology under license from the author(s). Two months after publication it is available to the public under an Attribution-Noncommercial-Share Alike 3.0 Unported Creative Commons License (<http://creativecommons.org/licenses/by-nc-sa/3.0>). "ASCB[®]," "The American Society for Cell Biology[®]," and "Molecular Biology of the Cell[®]" are registered trademarks of The American Society for Cell Biology.

formation of trans-SNARE complexes in exocytosis. In yeast, deletion of Sro7 and its redundant homologue, Sro77, causes secretory vesicles to accumulate in the emerging bud, whereas the actin cytoskeleton is unperturbed (Lehman *et al.*, 1999). This phenotype is similar to that of late secretory mutants and implicates that the Lgl/tomosyn family functions in polarized exocytosis rather than cytoskeletal regulation.

Recent evidence suggests that Sro7 could also act as a direct effector of Sec4 (Grosshans *et al.*, 2006). Sro7 was shown to bind to Sec4 in the presence of GTP and has genetic properties consistent with it functioning downstream of Sec4. However, there has not been rigorous testing that proves that the physical interaction with Sec4 is required for Sro7 function *in vivo*, so the mechanism of this interaction and whether it plays a role in exocytosis are unknown.

Sro7 is the only Lgl/tomosyn family member whose x-ray structure has been determined (Hattendorf *et al.*, 2007). In this study, we used the crystal structure of Sro7 to identify charged surface patches on Sro7 and screened for their involvement in the Sro7–Sec4 interaction. We combined these *in vitro* results with *in vivo* suppression studies and *in silico* modeling to validate the Sro7–Sec4 docking interaction interface. We found that disruption of the Sro7–Sec4 interaction results in a reduction of Sro7 function *in vivo*. Moreover, bioinformatic analysis suggests the possibility that the Sro7–Sec4 Rab-binding interface may be conserved in vertebrate tomosyn-1.

RESULTS

The interaction between Sro7 and the yeast Rab GTPase Sec4 is specific and GTP dependent

We showed previously that Sro7 binds preferentially *in vitro* to the GTP-locked conformation of the yeast Rab GTPase Sec4 (Grosshans *et al.*, 2006). More recently, Wang *et al.* (2011) reported an interaction between Lgl—the mammalian homologue of Sro7—and the Rab10 GTPase, which may play a role during axonal membrane protrusion. However, the biochemical analysis of this interaction suggests that Lgl and Rab10 interact in a GDP- rather than GTP-dependent manner. This further suggests that Lgl1 may act as

a GDP-dissociation inhibitor displacement factor facilitating the activation of Rab10 instead of as a Rab GTPase effector transducing the GTP-Rab function.

This prompted us to further examine nucleotide and Rab-binding specificity of Sro7 with the yeast Rab GTPases. We therefore examined binding properties of Sro7 with representatives of each subgroup of the well-characterized yeast Rab GTPase family (Lazar *et al.*, 1997; Buvelot Frei *et al.*, 2006; Lipatova *et al.*, 2015). Representatives of each of the eight yeast Rab subfamilies—Sec4, Ypt1, Ypt32, Ypt51, Ypt6, Ypt7, Ypt10, and Ypt11—were purified from *Escherichia coli* as N-terminally tagged glutathione S-transferase (GST) fusions, immobilized on glutathione Sepharose beads, and exchanged with guanosine 5′-3-O-(thio)triphosphate (GTPγS), GDP, or no nucleotide (Figure 1). As seen in Figure 1, purified full-length Sro7 binds specifically to GTPγS-Sec4 and fails to show significant binding to any of the other seven Rab proteins tested (Figure 1). Of importance, Sro7 binding is completely dependent on Sec4 being in a GTP-bound, activated state, and no detectable binding was seen to GDP or nucleotide-free forms of any of the eight Rab GTPases in yeast. Taken together, these results indicate that the interaction between Sro7 and the yeast Rabome is highly specific to Sec4 in its active or GTP-bound state.

Biochemical screen identifies two Sro7 mutants deficient in binding to Sec4-GTP

To begin to explore the molecular mechanism by which the Sec4 GTPase regulates Sro7, we set out to identify the site(s) of interaction between these proteins. The Sro7 is the only member of the Lgl/tomosyn protein family for which a high-resolution crystal structure has been determined (Hattendorf *et al.*, 2007). Sequence analysis based on close relatives of Sro7 combined with structural analysis identified a number of conserved surface patches as potential candidate sites on Sro7 for interaction with upstream regulators (*i.e.*, the Rab Sec4) or downstream targets of its function (*i.e.*, the target membrane SNARE [t-SNARE] Sec9). We focused our interrogation within each conserved patch on charged residues by creating

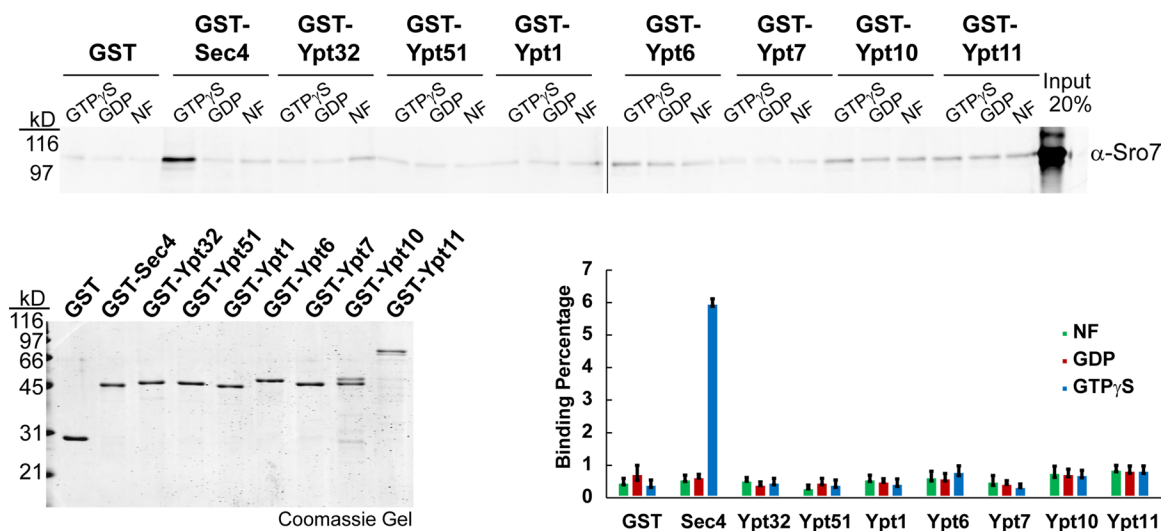


FIGURE 1: The interaction between Sro7 and the yeast Rab GTPase Sec4 is specific and GTP dependent. Soluble Sro7 was tested for binding to eight representatives of the yeast Rab GTPase family immobilized on glutathione Sepharose beads after exchange with GTPγS, GDP, or no nucleotide. Coomassie gel compares the amounts of Rab GTPases used in the *in vitro* binding. Quantitation is based on three independent experiments.

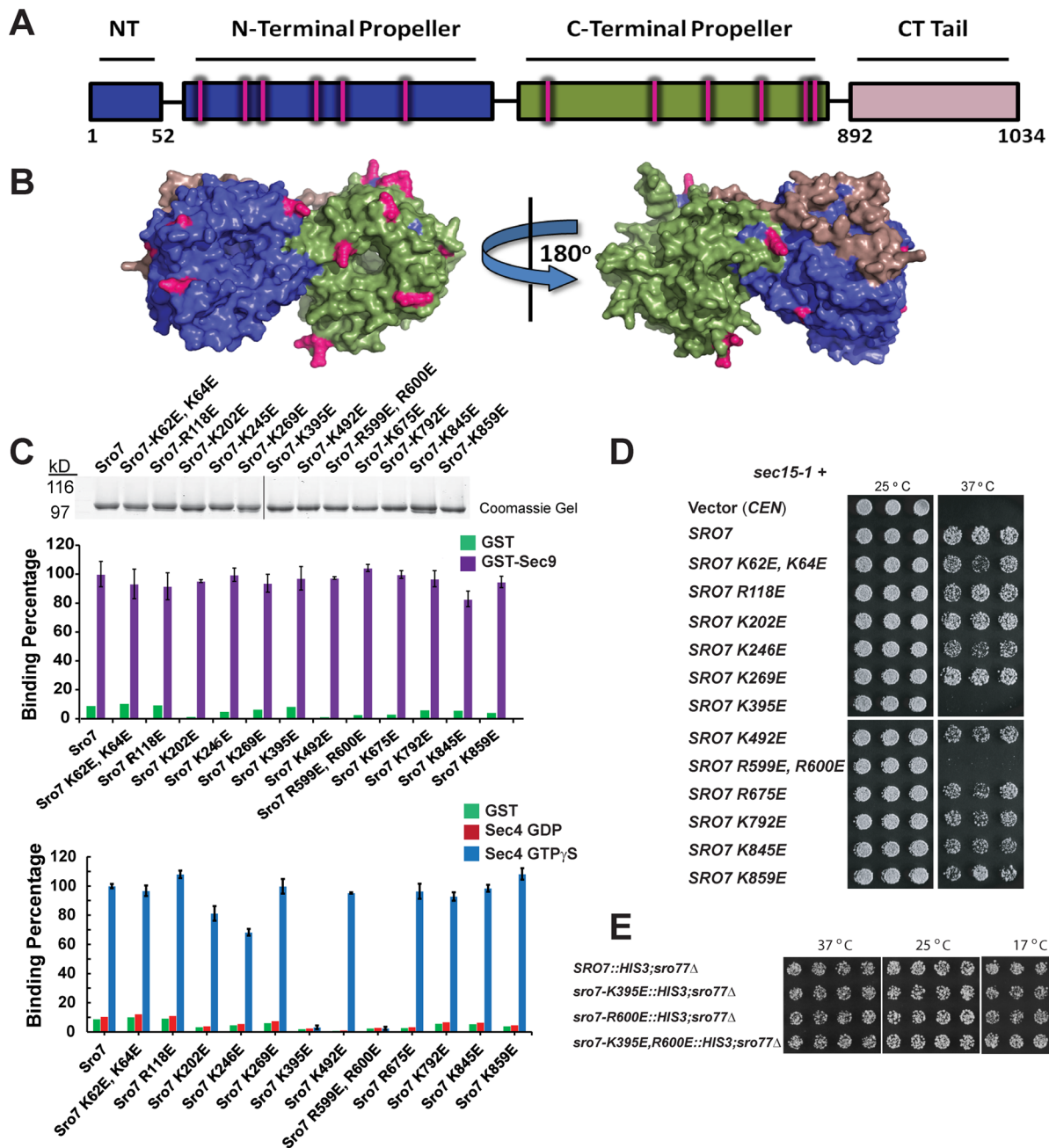


FIGURE 2: Biochemical screen identifies two Sro7 mutants deficient in binding to Sec4-GTP. (A) Schematic of Sro7 showing the N-terminal propeller in blue, the C-terminal propeller in green, and the autoinhibitory tail in light pink. Sites of charge-reversal mutations are indicated in fuchsia. (B) Surface-filling models of Sro7 showing the 12 residues subjected to mutation in fuchsia. (C) Coomassie gel of purified Sro7 and the Sro7 charge-reversal mutant proteins. Quantitation of Sro7 and Sro7 mutant protein binding to GST, GST-Sec9, or GST-Sec4 previously loaded with either GTP γ S or GDP. Binding was expressed as a percentage, with wild-type Sro7 binding set to 100%. Quantitation in each graph was based on four independent experiments. (D) The mutant strain *sec15-1* was transformed with a plasmid (CEN) expressing SRO7, the charge-reversal mutants, or vector only. Three independent transformants were picked into microtiter wells and transferred to YPD medium at 25 and 37°C. (E) Wild-type and SRO7 mutants unable to bind Sec4 were integrated as the sole source at the SRO7 locus. Four independent colonies were picked into microtiter wells and transferred to YPD medium at 37, 25, and 17°C.

charge-reversal mutations because of their high likelihood to disrupt protein–protein interactions. We therefore generated a collection of 12 different charge-reversal mutations that span both β -propeller domains of Sro7 and exclude known sites of interaction with the Sec9 N-terminus and with the regulatory tail of Sro7 (Figure 2, A and B; Hattendorf *et al.*, 2007). Wild-type Sro7 and the Sro7 mutants

were purified to homogeneity from yeast using a previously described multistep procedure (Rossi *et al.*, 2015), and all proteins were subjected to SDS–PAGE and Coomassie staining to assess both purity and quantity of each preparation (Figure 2C).

As a first examination of overall protein integrity, we compared wild-type Sro7 and the Sro7 mutant proteins for binding to a known

Sro7 ligand, the t-SNARE Sec9 (Lehman *et al.*, 1999). All 12 charge-reversal mutants bind GST-Sec9 comparably to wild-type Sro7, and statistical analysis of the binding data demonstrates that differences are not significant (Figure 2C).

To determine whether any of the 12 surface patches on Sro7 were involved in mediating specific binding to Sec4-GTP, we subjected each of the purified mutant proteins to binding assays with Sec4 that had been exchanged with GTP γ S or GDP. Of the 12 Sro7 mutant proteins, two—Sro7-K395E and Sro7-R599E, R600E—no longer bind to Sec4-GTP, and the remaining 10 bind Sec4-GTP at levels statistically similar ($p > 0.05$) to wild-type Sro7 (Figure 2C). None of the mutations has any detectable effect on the nucleotide specificity of the interaction with Sec4.

In parallel to the biochemical analysis of the surface patch mutants, we examined the effect of each mutation on *in vivo* function, using two distinct genetic assays. First, we examined the ability of the Sro7 mutants to function as the sole source of Sro7 in the cell. A double deletion in Sro7 (*sro7 Δ* , *sro77 Δ*) and its redundant homologue, Sro77, is cold sensitive and sensitive to salt, but one extrachromosomal copy of wild-type Sro7 complements this phenotype (Lehman *et al.*, 1999; Wadskog *et al.*, 2004). As the sole source of Sro7, all 12 of the charge-reversal mutants complement the cold and salt sensitivity of *sro7 Δ* , *sro77 Δ* like wild-type SRO7 (Supplemental Table I). To determine whether the lack of any detectable growth phenotype for the two Sec4-binding deficient mutants was related to the presence of the mutants on an extrachromosomal plasmid, we integrated each defective allele (*sro7-K395E* and *sro7-R600E*), as well as an allele with both mutations (*sro7-K395E,R600E*) into the native SRO7 locus by gene replacement (see Supplemental Figure S1 for details on the integration). The results of this analysis, shown in Figure 2E and Supplemental Figure S1, demonstrate that each of the single mutants is able to fully restore growth as the sole source of SRO7 at all temperatures and medium conditions examined, including 17°C and 0.7 M NaCl. Furthermore, the absence of a growth phenotype is unlikely due to residual binding present in each mutant, as the phenotype is identical to wild type even when both mutations are combined in a single allele (*sro7-K395E,R600E*).

The second genetic assay uses our previous observation that Sro7 plays a role as an effector of Sec4 that is parallel to the Exocyst complex, as overexpression of Sro7 strongly suppresses growth defects associated with deletions or temperature-sensitive mutations in subunits of the Exocyst complex (Lehman *et al.*, 1999; Zhang *et al.*, 2005; Grosshans *et al.*, 2006). Temperature-sensitive alleles of the Sec15 component of the Exocyst (*sec15-1*) are particularly sensitive to small increases in SRO7 dosage, as just a single additional copy (*CEN* plasmid) is sufficient to suppress temperature sensitivity of *sec15-1* at 37°C (Figure 2D). When the *sec15-1* suppression analysis was extended to the collection of surface patch mutants, we found that only the *sro7-K395E* and *sro7-R599E,R600E* alleles demonstrated loss of suppression. The other 10 surface patch alleles suppress *sec15-1* temperature sensitivity at levels comparable to wild-type SRO7. Taken together with the binding data in Figure 2C, these results identify a potential surface(s) on Sro7 involved in the interaction with Sec4 both *in vitro* and *in vivo*.

Computational docking studies extracted interacting elements from the best-scoring complexes of Sro7 and Sec4-GTP to produce four models

To examine the structural implications of the *in vitro* and *in vivo* effects of the described Rab binding mutants, we mapped the sites of the Sro7-K395 and Sro7-R599, R600 residues on the crystal structure

of Sro7. Of interest, these sites suggest that both the N-terminal and C-terminal β -propeller domains contribute to Sec4 binding and implicate a cleft formed by the intersection of the two propeller domains of Sro7 (Figure 3B). The identification of these novel Sro7 mutants piqued our interest in understanding the engagement between Sro7 and Sec4 in more detail. However, the relatively low affinity of the interaction between Sro7 and Sec4-GTP makes it unsuitable for analysis by cocrystallization experiments. Therefore we took an alternative approach that involved the combination of *in silico* docking studies with *in vitro* binding assays and *in vivo* suppression data to generate models for Sro7–Sec4 interaction. Like Sro7, the crystal structure of Sec4-GTP was previously determined (Stroupe and Brunger, 2000). We used the ClusPro 2.0 docking program to perform docking simulations between Sro7 and Sec4. The simulations filtered conformations for low desolvation and electrostatic energies and ranked poses by cluster size for the best-scoring protein–protein complexes. The results revealed that four of the high-scoring models include the involvement of Sro7 residues K395 and R599 or R600 in the *in silico* interaction with Sec4-GTP (shown in red, Figure 3B), which is consistent with the given *in vitro* binding data. In addition, all four models implicate one or both of the switch I and II regions of Sec4, which are the structural elements of Ras GTPases that change in response to the nucleotide state and are therefore strongly predicted to be involved in the interaction with an Sec4 effector protein such as Sro7.

All four Sro7–Sec4 docking models included the same Sro7 interface for Sec4 binding (Figure 3A). This region is in a pocket on the opposing side of the protein from where the Sro7 regulatory tail and the t-SNARE Sec9 bind. To confirm that this Sro7 interface is involved in binding to Sec4 as predicted by these four docking models and further delineate the site of Sec4 binding on Sro7, we created a second set of Sro7 mutants at this interface (shown in orange, Figure 3B). We characterized the Sro7 mutants both *in vitro* by binding to Sec4-GTP and *in vivo* by analysis of their ability to suppress the growth defect of *sec15-1* at 37°C. The results, shown in Figure 3C, demonstrate that two of the three mutant proteins—Sro7-D326R and Sro7-S327A, T329E—are deficient in binding to Sec4-GTP, whereas Sro7-D361K binds Sec4-GTP comparably to wild-type Sro7. Similarly, when we examined the Sro7 mutants *in vivo* by testing their ability to suppress the temperature sensitivity of *sec15-1*, we found that the same two mutants that are deficient in binding to Sec4-GTP—*sro7-D326R* and *sro7-S327A, T329E*—are also unable to suppress growth at the restrictive temperature (Figure 3C). Also consistent with the binding data, *sro7-D361K* suppresses *sec15-1* at 37°C similarly to wild-type SRO7 suppression (Figure 3C). As with our previous Sec4-binding mutants, these alleles show no obvious growth defects as the sole source in complementation of the severe cold-sensitive growth defect present in the *sro7 Δ* , *sro77 Δ* double-deletion strain (Supplemental Table I). The results of this characterization support the prediction that the Sro7 interface incorporated in the four docking models is highly likely to be a component of the binding site for Sec4-GTP. Moreover, these results are consistent with the previous finding in Figure 2 that Sro7 mutants unable to bind Sec4-GTP also demonstrate a clear defect *in vivo* to overcome the loss in Exocyst complex function present in *sec15-1*.

Novel mutations in Sec4 were designed to discriminate among predicted *in silico* docking models

Although the same binding interface of Sro7 is involved in all four docking models, the orientation of Sec4 with respect to Sro7 is substantially different in each model (Figure 4A). We therefore generated a second set of mutations in surface-exposed, charged Sec4

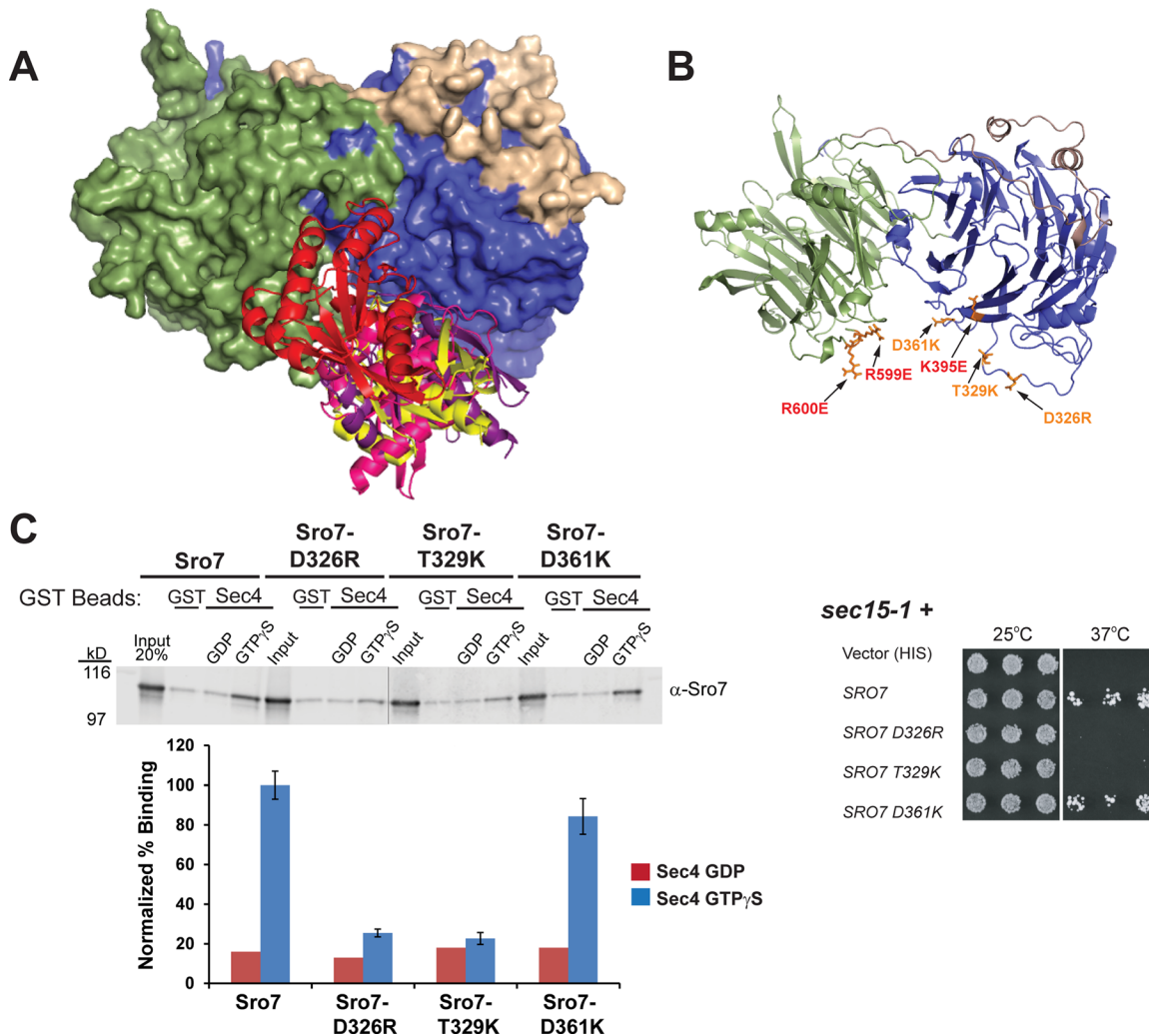


FIGURE 3: Computational docking studies extracted interacting elements from the best-scoring complexes of Sro7 and Sec4-GTP to produce four models. (A) Surface-filling model of Sro7 with an overlay of the four Sec4 docking arrangements. The Sro7 N-terminal propeller is shown in blue, the C-terminal propeller is in green, and the C-terminal tail is in light pink. The Sec4 ribbon diagrams (models A–D) are colored in yellow, pink, red and purple, respectively. (B) Ribbon diagram of Sro7, with new mutations at the Sro7–Sec4 interface marked in orange. Original mutations are marked in red. (C) Purified wild-type Sro7 or Sro7 mutants were tested for binding to GST–Sec4 after exchange with either GTP γ S or GDP. Western blot and quantitation from four independent experiments. The mutant strain *sec15-1* was transformed with a plasmid (*CEN*) expressing *SRO7*, the novel discriminatory mutants, or vector only. Three independent transformants were picked into microtiter wells and transferred to YPD medium at 25 and 37°C.

residues with the aim of distinguishing among the four models. To accomplish this, we chose six residues to mutate with high predictive value in distinguishing among the four models based on differences in their predicted distance from Sro7 in the four models. Residues were scored for high interaction potential when the distance was $<4 \text{ \AA}$ and low interaction potential when the distance was $>4 \text{ \AA}$ (Figure 5A). For example, the Sec4-D56R mutant is predicted to be involved in Sec4–Sro7 docking in models A, C, and D but not in model B. Therefore this particular mutation will discriminate model B from the other models. The locations of the novel set of Sec4 mutations tabulated in Figure 5A are shown by a ribbon diagram in Figure 4B.

Wild-type Sec4 and the discriminatory Sec4 mutants were purified as GST fusion proteins, exchanged with either GTP γ S or GDP, and tested for binding to wild-type Sro7. The binding data shown in Figure 4C demonstrate that four of the six mutant proteins tested

exhibit a significant defect in binding to Sro7, whereas two of the mutant Sec4 proteins bind to Sro7 at levels similar to that for wild-type Sec4. To analyze the in vivo consequences of Sec4 mutations resulting in a loss of binding to Sro7, we used the fact that, like *SRO7*, one additional copy of *SEC4* (on *CEN*) strongly suppresses the temperature sensitivity of a *sec15-1* strain (Salminen *et al.*, 1987). As can be seen in Figure 4C, all four of the mutant alleles of *SEC4* that encode proteins defective in binding to Sro7 in vitro also have completely lost the ability to suppress the *sec15-1* mutant temperature sensitivity. Similarly, the two mutant *SEC4* alleles that encode proteins that bind to Sro7 at levels similar to that of wild-type Sec4 also demonstrate suppression of *sec15-1* temperature sensitivity in a manner indistinguishable from that of wild-type *SEC4*. The strong correlation between the biochemical and genetic analyses strongly supports the notion that the interaction between Sec4 and Sro7 observed in vitro is also important for the function of both proteins within the cell.

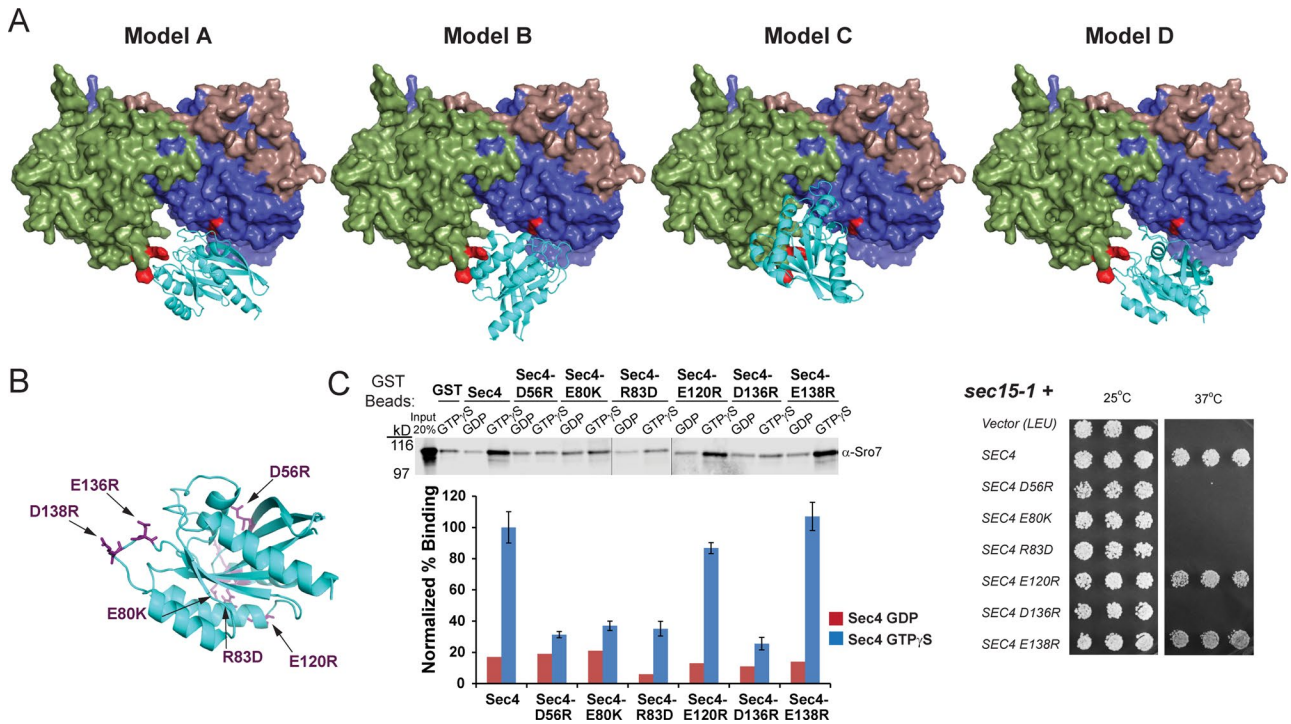


FIGURE 4: Novel mutations in Sec4 were designed to discriminate between predicted in silico docking models. (A) In the surface-filling models (A–D) of Sro7, the N-terminal propeller is shown in blue, the C-terminal propeller in green, and the C-terminal tail in light pink. The Sro7 mutations defective in binding Sec4-GTP (cyan) are shown in red. (B) Ribbon diagram of Sec4-GTP, with discriminatory mutations in purple. (C) Wild-type Sec4 or Sec4 mutants were purified as GST fusion proteins and bound to Sro7 as previously described. Western blot of binding and quantitation from four independent experiments. *Sec15-1* was transformed with a plasmid (CEN) expressing *SEC4*, the discriminatory mutants, or vector only. Three independent transformants were picked into microtiter wells and transferred to YPD medium at 25 and 37°C.

We next examined whether the binding and suppression data would allow us to discriminate among the four docking arrangements. We compiled the tabulated predicted effects of the Sec4 mutations on Sro7–Sec4 binding for each of the four models based on the distance of the mutated residue from the Sro7 binding interface (Figure 5A). As previously stated, low interaction potential (marked with a minus sign in Figure 5A) corresponds to mutated Sec4 residues at a distance >4 Å from Sro7, and high interaction potential (marked with a plus sign in Figure 5A) corresponds with mutated Sec4 residues at a distance of <4 Å from Sro7. Based on the in vitro and in vivo studies, mutations that blocked both Sro7 binding and *sec15-1* suppression are indicated with an asterisk, and those mutations that had no effect on binding and suppression are unmarked (Figure 5A). In interpreting these results, it is important to note that it is possible for a residue to be predicted within 4 Å of the interface and still not affect binding when mutated. However, when a mutated residue is >4 Å from the binding interface in a particular docking model, there is a strong prediction that the mutated residue will have no effect on the observed in vitro interaction and in vivo suppression analyses. For example, in docking models A and B, Sec4-E80K is predicted to be >4 Å from the binding interface on Sro7, yet this mutant dramatically affected the Sro7–Sec4 interaction both in vitro and in vivo. Therefore it is unlikely that models A and B are the correct docking arrangements between Sro7 and Sec4, and this is scored as an inconsistency (in red) in Figure 5A. As can be seen, models A–C all contain several inconsistencies with regard to comparison of predicted effects of mutations with effects observed in vitro and in vivo. In contrast, model D (Figure 5B) is the sole model with perfect correlation between its interaction predic-

tions and the actual in vitro and in vivo data (Figure 5A). In addition, four of the five mutated Sec4 residues in model D are predicted to be within 4 Å of the Sro7–Sec4 binding interface and demonstrate a strong effect on both binding and suppression.

Three distinct patches of mutations on both proteins affecting the Sro7–Sec4 interaction correspond nicely between Sro7 (orange residues) and Sec4 (purple residues): Sro7-R599E, Sro7-R600E, and Sec4-D136R on the C-terminal β-propeller front side of the binding cleft (Figure 5, bottom inset), Sro7-K395E and Sec4-D56R on the N-terminal β-propeller front side of the binding cleft (Figure 5, bottom inset), and Sro7-D326R, Sro7-T329K, Sec4-E80K, and Sec4-R83D on the N-terminal β-propeller back side of the binding cleft (Figure 5, right inset). On the basis of this extensive analysis, we invalidated three of the four docking models and have substantial evidence that model D is the native docking arrangement for interaction between Sro7 and Sec4-GTP.

How does Sro7 selectively bind GTP-bound Sec4?

The results shown in Figure 1 demonstrate that Sro7 has the biochemical properties of a Rab effector with high substrate specificity for Sec4, as we do not detect Sro7 interaction with any other Rab GTPase in yeast. In addition, the Sro7–Sec4 interaction is highly specific to the GTP-bound or activated form of Sec4. Our determination of a well-validated, high-resolution model for Sro7–Sec4 docking allows us to identify elements of the binding interaction that are likely responsible for these two effector-specificity aspects of Sro7 with Sec4. Close examination of the model illustrates four regions within Sec4 that are in most intimate contact with Sro7 (Figure 6). Two of the regions in close contact with Sro7 are the switch I and

A

Docking Model Interaction Prediction				
Sec4 Mutants	Model A	Model B	Model C	Model D
* D56R	+	-	+	+
* E80K	-	-	+	+
* R83D	-	+	-	+
E120R	-	+	-	-
* D136R	+	-	-	+
E138R	+	-	+	+
Inconsistencies:	2	3	2	0

B

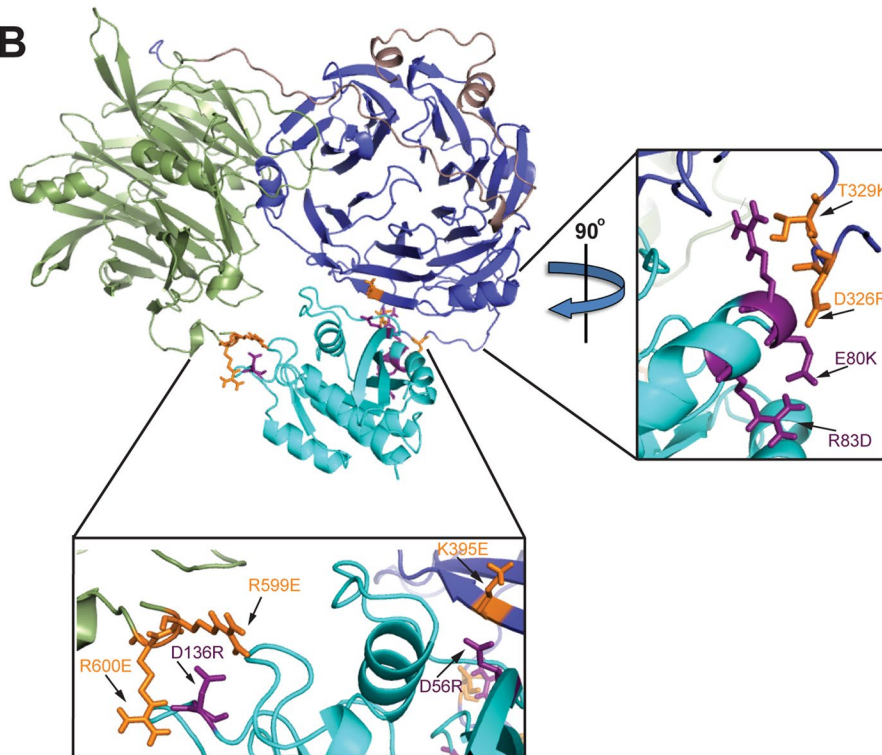


FIGURE 5: Mutations in Sec4 predict a precise model for the docking of Sec4 onto the binding cleft of Sro7. (A) Table of interaction predictions for Sec4 discriminatory mutations specific to each docking model based on their distance from Sro7. Distances $>4 \text{ \AA}$ were scored as a low interaction prediction (–), and distances $<4 \text{ \AA}$ were scored as a high interaction prediction (+). Based on *in vitro* and *in vivo* characterization, mutations that affected the interaction are indicated with an asterisk. Results inconsistent with the initial interaction prediction are indicated in red. (B) Validated docking interaction between Sro7 and Sec4-GTP. Sro7 residues involved in the interaction are shown in orange. Sec4 residues involved in the interaction are shown in purple. Insets are enlargements of docking site straight on (bottom inset) and at a 90° rotation (right inset).

switch II domains of Sec4—the two regions that undergo the most conformational change when comparing GDP and GTP-bound structures, which are therefore critical to nucleotide-specific recognition of small GTPases by effectors and accessory proteins (Vetter and Wittinghoffer, 2001). The four Sro7 contact regions within Sec4 are residues 46–58 (the entire switch I domain), residues 79–84 (within the switch II domain), Sec4-135–140, and Sec4-162–167. The first two regions make contact with the Sro7 N-terminal β -propeller domain; the latter two interact with the Sro7 C-terminal β -propeller domain.

To determine which of these four regions is likely used by Sro7 to distinguish Sec4 from other Rab GTPases in yeast, we examined sequence alignments of the eight yeast Rab family members used in Figure 1—Sec4, Ypt1, Ypt31, Vps21, Ypt10, Ypt6, Ypt7, and Ypt11.

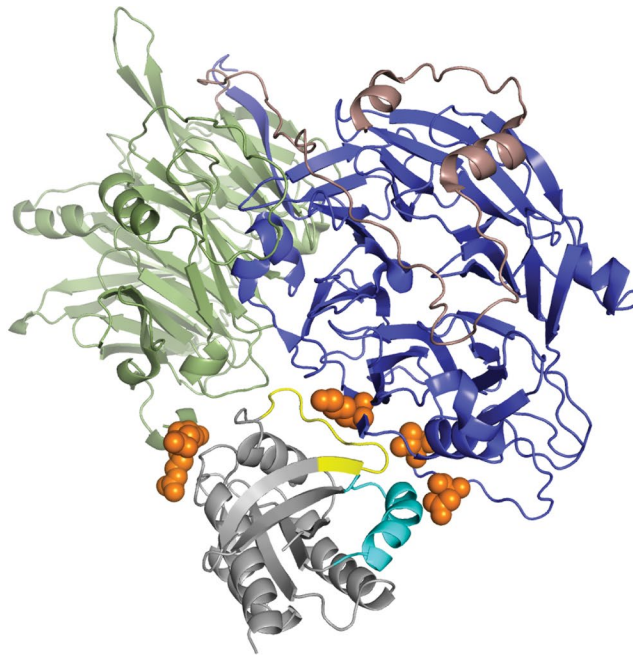
function is shared between yeast and vertebrate homologues (Sakisaka *et al.*, 2004), it is possible that the Rab effector function is also shared with one or more of the vertebrate homologues. If so, one might expect to see reduced surface variability within the region predicted to form the homologous Sro7–Sec4 binding cleft. We therefore used a combined structural and phylogenetic approach to examine the surface variability of vertebrate members of tomosyn and Lgl, especially within the region homologous to where Sec4 interacts with Sro7. We used the MODELLER program to build structural models of tomosyn-1 and Lgl-1, using the crystal structure of Sro7 as a template. The tomosyn-1 model is similar to that made by Williams *et al.* (2011). We then mapped onto the models invariant residues identified from multiple sequence alignments. A multiple sequence alignment of 16 Sro7 homologues from the

We found that the Sro7-interacting region within the Sec4 switch II domain is highly conserved within the yeast Rabome (Figure 6). Therefore the interaction of Sro7 with the switch II domain of Sec4 is unlikely to be involved in mediating Rab specificity but instead likely plays a role in determining the nucleotide-binding-state specificity of the protein. Like the switch II domain, the C-terminal half of the Sec4 switch I domain (residues 52–58) is also highly conserved among the yeast Rab GTPases (Figure 6). In contrast, the first six residues of the switch I domain (residues 46–51) of Sec4 are quite distinct from those of the homologous switch I domains in the other yeast Rabs (Figure 6, dark blue residues boxed in yellow). In fact, of the four contact sites in our model used by Sro7 to bind Sec4, only this segment of the Sec4 switch I domain demonstrates the kind of variability that one would expect of a site responsible for the Sro7 substrate specificity. Taking the results together, we conclude that whereas Sro7 contact with both the switch I and switch II domains is likely responsible for recognition of the GTP-bound state of Sec4, it is the specific interaction with the N-terminal segment of the switch I domain that provides the high degree of Rab specificity for recognition of Sec4-GTP by the Sro7 effector protein.

Conservation of the Sro7–Sec4 binding interface within the Lgl family of proteins

Structural and evolutionary examination of surface residue variation has demonstrated that protein–protein interfaces are significantly more constrained in their variability than are noninteraction surfaces (Levin *et al.*, 2009; Dey *et al.*, 2010). Structural alignments of Sro7 with its closest vertebrate homologues, tomosyn and Lgl, demonstrate that the overall dual- β -propeller domain structure of Sro7 is likely shared by all three members of this family (Hattendorf *et al.*, 2007). Because the SNARE regulatory

A



B

		Switch I		Switch II	
SEC4	43	DKFNPSFIT TIGIDF KIKTVDING-----KVKVLQLWDTAG QERFR -TITTAYYRGAMGIILVYDVTD	104		
YPT1	31	DTYTNDYIS TIGVDF KIKTVELDG-----KTVKLQIWDTAG QERFR -TITSSYYRGSHGIIIVYDVTD	92		
YPT31	36	NEFN NMDSKS TIGVEF ATRTRLEIDG-----KRIKAQIWDTAG QERYR -AITSAYYRGAVGALIVYDISK	97		
VPS21	30	NDF AE NKE P TIGAAF LTQRVTIN-----EHTVKFEIWDTAG QERFA -SLAPMYRQAALVVYDVTK	91		
YPT10	27	GKFL LAKHAA TIGAAF ITTKTIEVPSNDSSTEKRIHMEIWDTAG QERYK -SLVPMYYRDANIALIVFELGD	94		
YPT6	33	DTE DDHYQA TIGIDF LSKTMVLD-----DKTIRLQLWDTAG QERFR -SLIPSYIRDSRVAVIIVYDITK	94		
YPT7	31	DKYS SQYKA TIGADF LTKEVTVDG-----DKVATMQVWDTAG QERFQ -SLGVAFYRGADCCVLVYDVTN	93		
YPT11	196	NEI VIETRS TIGIDI KTNLVNIDN-----RFFNVILWDTAG QERYQNAI IPSLYKKTNAVILTYDITN	258		

Variable
 Conserved

FIGURE 6: Sec4 effector specificity for Sro7 interaction is attributed to the Sec4 N-terminal half of the switch I domain. (A) Crystal structure of Sro7 docked with Sec4-GTP (gray). The N-terminal propeller is blue, the C-terminal propeller is green, and the autoinhibitory tail is light pink. Ribbon diagram of Sec4 is shown with the switch I domain in yellow (residues 48–56) and the switch II domain in cyan (residues 76–93). Sro7 residues involved in the interaction are shown in orange. (B) Multiple sequence alignments were performed using ClustalX with each of the eight yeast Rab family member representative proteins (Ypt1, Ypt31, Vps21, Ypt10, Ypt6, Ypt7, and Ypt11). The Sec4 switch I sequence is boxed in yellow, and the Sec4 switch II sequence is boxed in cyan. Switch domain residues within 4 Å of Sro7 are highlighted as either highly variable (dark blue) or highly conserved (light red) for the eight yeast Rab proteins.

Saccharomycetaceae family, one family of budding yeast, was used for comparison (Figure 7, left). Invariant residues were also identified from an alignment of 47 tomosyn-1 vertebrate (fish, frog, bird, and mammal) homologues (Figure 7, middle) and from 34 Lgl-1 vertebrate homologues (Figure 7, right). Conserved invariant residues are indicated in pink on the Sro7 crystal structure and the tomosyn and Lgl structural models, respectively (Figure 7). Although rates of surface change are overall much greater in the yeasts compared with vertebrates (presumably due to both functional redundancy with the Exocyst complex and much shorter generation time), specific sites of low variability are apparent in all three family members.

There are three areas on the surface of Sro7 with decreased variability within the yeast family: regions homologous to where the Sro7 regulatory tail binds back to the N-terminal β-propeller, the binding site for the N-terminus of the t-SNARE Sec9 (Hattendorf *et al.*, 2007), and residues within the Sro7–Sec4 binding pocket (Figure 7). When we focus specifically on the Sec4 binding cleft on Sro7, the variability among the yeast members reveals two con-

served sites in the Sro7–Sec4 binding pocket—one on the C-terminal β-propeller including the Sro7-R600 residue and one on the N-terminal β-propeller including the Sro7-K395 residue (Sro7 inset, Figure 7). Residues Sro7-R600 and Sro7-K395 were previously shown to be directly involved in the Sro7–Sec4 interaction (Figure 2). The conserved Sro7-K395 area in the docked Sro7–Sec4 structure interacts with the Sec4 switch I domain (yellow), the region of Sec4 responsible for effector specificity, consistent with the correlation between decreased protein surface variability and functional importance (Sro7 inset, Figure 7).

Human tomosyn-1 and Lgl-1 protein sequences were used to build structural models based on the Sro7 crystal structure template. As with the yeast family members, invariant surface residues within tomosyn and Lgl vertebrate homologues were mapped onto the structural models of tomosyn-1 and Lgl-1. In contrast to yeast, tomosyn family members have several conserved regions spanning both faces of its dual-propeller structure, likely attributed to increased surface fixation from acquired functionality (Figure 7). Like tomosyn, Lgl vertebrates also

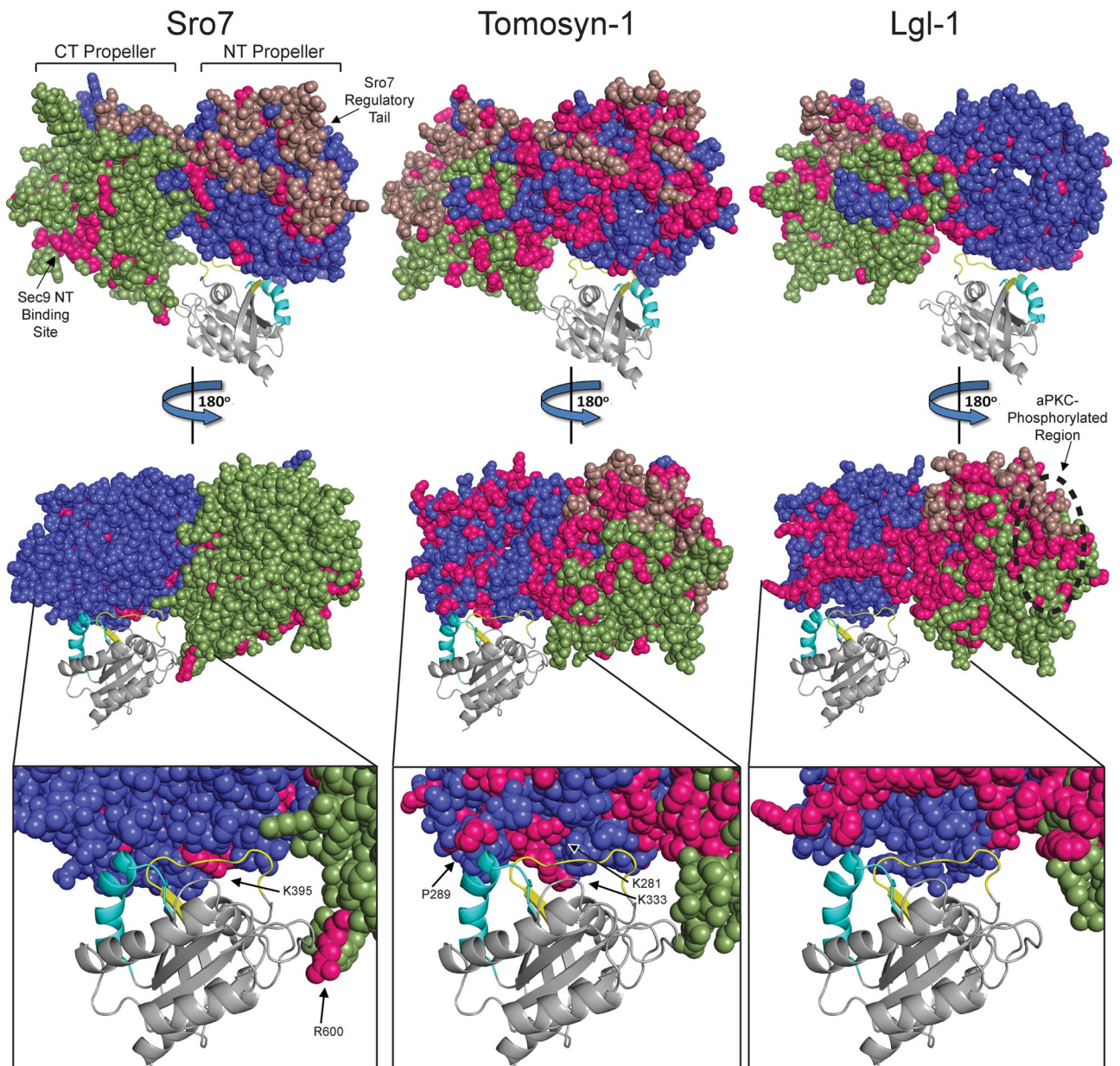


FIGURE 7: Conservation of the Sro7–Sec4 binding interface within the Lgl family of proteins. Crystal structure of Sro7 (left) and structural models of tomosyn-1 (middle) and Lgl-1 (right) docked with Sec4-GTP (gray). Structural models were built with MODELLER, using the crystal structure of Sro7 as a template. The tomosyn-1 model is similar to that shown by Williams *et al.* (2011), except that unstructured insertions are omitted from the structural models shown. The N-terminal propeller is blue, the C-terminal propeller is green, and the regulatory tail is light pink. Ribbon diagrams of Sec4 are shown with the switch I domain in yellow and the switch II domain in cyan. Invariant residues were identified from three multiple sequence alignments. One alignment was of 16 Sro7 homologues from the Saccharomycetaceae family of budding yeast, a second of 47 tomosyn-1 vertebrate homologues, and a third of 34 Lgl-1 vertebrate homologues. Sites of invariant conserved residues are indicated in pink on corresponding structures. Structures flipped vertically 180° were also slightly rotated horizontally 30° to better view the binding pocket. Insets are enlargements of homologous Sro7–Sec4 binding site straight on. The Sro7 C-terminal tail and Sec9 N-terminus binding sites are indicated in the Sro7 crystal structure (top left). Conserved Sro7 residues involved in the Sro7–Sec4 interaction are indicated in the Sro7 inset (left inset). Invariant tomosyn-1 residues that correspond with the Sro7-K395 site are indicated in the tomosyn-1 model (middle inset). The aPKC-phosphorylated residues on Lgl are within one of the omitted unstructured insertions. This region is indicated in the Lgl-1 structural model (middle right).

developed greater surface residue conservation; however, the invariant residues are located primarily on one protein face—the same face where the aPKC phosphorylation sites reside (Figure 7). A focused examination of the region of tomosyn that is homologous to the Sro7–Sec4 binding pocket reveals that verte-

brate tomosyn-1 family members maintain significant conservation within the interaction interface. Of note, there is a cluster of invariant residues in tomosyn-1 that corresponds to the part of the binding cleft in Sro7 containing the critical K395 residue (tomosyn inset, Figure 7).

Of interest, the surface conservation in vertebrate Lgl-1 members is quite distinct from the conservation observed in vertebrate tomosyn-1 proteins. Whereas there is a significant increase in overall Lgl surface residue conservation compared with Sro7 and tomosyn-1, the region corresponding to the Sec4 binding pocket in Sro7 is significantly more variable in Lgl-1 (Lgl inset, Figure 7). This suggests that of the two vertebrate branches of the Sro7/Lgl/tomosyn family, tomosyn is the most likely to have a conserved role as an effector for a vertebrate Rab GTPase.

DISCUSSION

This study describes for the first time the structural details of the Sec4 GTPase interaction with a direct downstream effector, Sro7. Whereas previous work detailed the interaction between Sro7 and its downstream t-SNARE target, Sec9, this study gives the first structural clues as to how a member of the Lgl/tomosyn/Sro7 family of proteins is engaged by a Rab GTPase. One of the defining characteristics of the Lgl/tomosyn/Sro7 family is the central structure composed of two adjacent seven-bladed β -propellers having extensive interactions between the N- and C-terminal propellers (Hattendorf et al., 2007). Here we map the binding site used by the Sec4 GTPase in its interaction with Sro7 to a cleft formed at the intersection of these two propellers—an interaction that is highly specific to the yeast Rab family member Sec4 in its activated, GTP-bound form.

Our bioinformatic analysis of the sequence variation found in vertebrate members of the tomosyn1/2 family suggests that this cleft may also be important for the interaction between tomosyn and a related small GTPase, perhaps as part of an ancestral function for this family of proteins that predates the divergence of the family members (Fasshauer and Jahn, 2007; Klopper et al., 2008). Of interest, there is significantly less conservation in the homologous Sro7–Sec4 binding interface for members of the Lgl1/2 family than for tomosyn1/2. We can only speculate about the precise significance of this difference, but it could be attributed to divergence or loss of the ancestral Rab effector function as the Lgl family evolved distinct functions from tomosyn in metazoans. This functional separation between family members could have occurred in parallel to the loss of the C-terminal R-SNARE motif in members of the Lgl family in metazoans (Fasshauer and Jahn, 2007). Of interest, Wang et al. (2011) reported a direct interaction between Lgl1 and the Rab10 GTPase. However, unlike the GTP-dependent Sro7–Sec4 interaction, Lgl1 appears to interact specifically with the GDP- rather than GTP-bound form of Rab10.

A surprising aspect of this study arose when we were investigating the importance of interaction with the Sec4 GTPase to the in vivo function of Sro7 within the cell. Although there is an absolute requirement for Sro7–Sec4 interaction to rescue the late secretory mutant *sec15-1*, mutant forms of Sro7 that are unable to bind Sec4-GTP, show no detectable growth or secretion defect when present as the sole source of *sro7* and *sro77* in the cell (Supplemental Table I). The simplest explanation for this behavior is that Sro7 function overlaps significantly with the function of the Exocyst complex as part of a dual or parallel effector pathway. The Exocyst and Sro7 were both shown to bind directly to Sec4-GTP and have SNARE regulatory properties (Grosshans et al., 2006; Hattendorf et al., 2007; Heider et al., 2012). In fact, overexpression of Sro7 suppresses a number of mutations and deletions in components of the Exocyst and has genetic properties consistent with a parallel function (Lehman et al., 1999; Grosshans et al., 2006). Further work will allow us to determine more precisely which aspects of the Sec4/Sro7 effector pathway (vesicle tethering vs. SNARE assembly) represent elements functioning in parallel to those of the Exocyst complex

and which aspects are unique to Sro7 or the Exocyst in carrying out Sec4's essential functions in exocytosis (Grosshans et al., 2006; Rossi et al., 2015).

MATERIALS AND METHODS

Media and reagents

Yeast growth media used in this study include 1% bacto-yeast extract, 2% bacto-peptone, 2% dextrose (YPD; Difco, Sparks, MD), S minimal (0.67% yeast nitrogen base without amino acids and 2% dextrose; Difco), agar (Fisher Scientific, Pittsburgh, PA), and dropout media (0.67% yeast nitrogen base without amino acids, synthetic complete amino acid supplement minus appropriate amino acid(s), and 2% dextrose; US Biological, Swampscott, MA).

Bacteria growth media used in this study include Terrific Broth (4.7% bacto-TB, 1% glycerol; Fisher Scientific), Super Optimal Broth (SOB; 2% tryptone; Difco), 0.5% bacto-yeast extract, 2.5 mM KCl (Sigma-Aldrich, St. Louis, MO), 1 M NaCl, 10 mM MgCl₂, and 10 mM MgSO₄ (Fisher Scientific), SOB with catabolite repression (SOB + 2.5% glucose), and lysogeny broth (1% bacto-tryptone, 0.5% bacto-yeast extract, and 1% NaCl).

Reagents used in this study were as follows: GTP γ S, Triton X-100, GDP, sodium azide, sodium fluoride, dithiothreitol (DTT), β -mercaptoethanol, pepstatin A, and leupeptin 1 mg/ml, aprotinin 2 mg/ml, and antipain 1 mg/ml were obtained from Sigma-Aldrich. Ampicillin and 4-(2-aminoethyl) benzenesulfonyl fluoride were obtained from US Biological. Tween-20 and Broad Range Protein Standard were obtained from Bio-Rad (Hercules, CA). Glutathione Sepharose 4B, Protein A Sepharose, and Precision Protease were obtained from GE Healthcare (Milwaukee, WI). Secondary antibodies for the Odyssey Imaging System are from LI-COR Biosciences (Lincoln, NE) and Molecular Probes (Eugene, OR). 5-Fluoroorotic acid was obtained from Thermo Scientific (Waltham, MA). Immunoglobulin G Sepharose 6 Fast Flow beads were obtained from Amersham Biosciences (Piscataway, NJ).

Yeast strains and genetic analysis

The yeast strains that were constructed and used for this study are listed in Supplemental Table II. Yeast transformations were performed using the lithium acetate method (Moerschell et al., 1991). For genetic analysis, at least three different spores were analyzed per experiment.

Plasmids and molecular biology

The plasmids that were constructed and used for this study are listed in Supplemental Table III. Sro7 charge-reversal mutants were generated by site-directed mutagenesis on pB2129 (Sro7, *CEN*, *HIS3* plasmid). Protein A–tagged Sro7 constructs were generated as *Bam*HI/*Hind*III subclones in pB966 (Protein A, 2 μ plasmid) as previously described (Rossi et al., 2015). Sro7 charge-reversal mutants were generated by site-directed mutagenesis on pB1931 (Sec4, *CEN*, *LEU2* plasmid). GST-tagged Sec4 constructs were generated as *Bam*HI-*Sall* fragments in pB 2173 (pGEX-6P1 plasmid). GST-tagged Rab protein constructs were generated using genomic DNA as *Bam*HI-*Sall* fragments (Ypt32, Ypt51, Ypt1, Ypt6, Ypt7, Ypt10) or *Bgl*II-*Sall* (Ypt11) fragments and subcloned into pB 2173 (pGEX-6P1 plasmid). Constructs were confirmed by sequencing.

Protein purification

Wild-type Sro7 and Sro7 charge-reversal mutant proteins were purified as previously described (Rossi et al., 2015). GST fusion proteins (Sec4, Sec4 charge-reversal mutants, Ypt32, Ypt51, Ypt1, Ypt6, Ypt7, Ypt10, and Ypt11) were transformed into BL21 *E. coli* and expressed

as previously described (Grosshans *et al.*, 2006). Sec9 with a C-terminal hexahistidine tag was purified from *E. coli* as previously described (Gangar *et al.*, 2005).

In vitro binding assays

In vitro binding of wild-type Sro7 and Sro7 charge-reversal mutants to GST fusions of Sec9, Sec4, Sec4 mutants, and the seven Rab family proteins was performed using previously described conditions (Grosshans *et al.*, 2006) with the following modifications. During nucleotide exchange, beads were incubated with 100 μ M GTP γ S or GDP or nucleotide free for 30 min at 25°C. After this incubation, MgCl₂ was added to a final concentration of 30 mM and incubated for 1 h at 25°C. Binding buffer consisted of 20 mM Tris-HCl, pH 7.4, 140 mM NaCl, 10 mM MgCl₂, 1 mM DTT, and 0.5% Triton X-100. In vitro binding of wild-type Sro7 and Sro7 charge-reversal mutants to GST-Sec9 (full length) was performed using previously described conditions (Gangar *et al.*, 2005). Binding percentages for all in vitro binding experiments were expressed as percentage of binding relative to wild-type Sro7 binding. The *p* values were determined using Student's *t* test from three separate binding experiments for each protein.

Protein–protein docking analysis

Docking simulations between Sro7 and Sec4 were performed with the automated docking server ClusPro 2.0 (Comeau *et al.*, 2004), using solved crystal structures for Sro7 (Hattendorf *et al.*, 2007; Protein Data Bank [PDB] Code 2OAJ) and for GTP-Sec4 (Stroupe and Brunger, 2000; PDB Code 1G17). We did not use the advanced option of attractive residues to drive the complex toward the regions of interest on Sro7 and Sec4 during the ClusPro docking calculations. ClusPro results were refined complex structures based on the largest clusters of poses that represent the most likely protein–protein interactions. We analyzed the top 10 clusters for each of four scoring functions provided: 1) Balanced, 2) Electrostatic-favored, 3) Hydrophobic-favored, and 4) VdW+Electrostatic. The 40 ClusPro complexes were analyzed for docking poses that placed D56 of switch I and/or E80 of switch II of GTP-Sec4 near Sro7 residues R599/R600 and/or K395. From the 40 docking poses, the top 10 poses for each of the four scoring functions included nine poses that involved both the Sec4 and Sro7 residues of interest. These nine poses could be separated into four unique poses, as some poses were identified as large clusters for more than one scoring function. A contact analysis for residues in Sec4 within 4 Å of Sro7 interface residues was calculated using PyMOL tools (Jones *et al.*, 2012).

Tomosyn-1 and Lgl-1 model building

The sequences for human tomosyn-1 and Lgl-1 were submitted to the HHpred fold recognition server (toolkit.tuebingen.mpg.de/hhpred). The 14 WD-repeat structure of yeast Sro7 was identified as a top hit. The models of tomosyn-1 and Lgl-1 were built using MODELLER (Eswar *et al.*, 2006) based on the yeast Sro7 (PDB ID 2OAJ) template.

Sequence analysis

Sequences for vertebrate tomosyn-1 and for tomosyn homologues in the hemichordate acorn worm (*Saccoglossus kowalevskii*) and the echinoderm purple sea urchin (*Strongylocentrotus purpuratus*) were identified using BLAST (Altschul *et al.*, 1990) and aligned in ClustalX (Higgins and Sharp, 1988; Thompson *et al.*, 1997). A similar procedure was followed for Lgl-1 homologues in vertebrates and the higher metazoans.

ACKNOWLEDGMENTS

We thank Mallory Demonch for assistance in generating plasmids and reagents used in this work. This work was supported by National Institutes of Health Grants GM-054712 and P30-CA016086.

REFERENCES

- Aalto MK, Ronne H, Keranen S (1993). Yeast syntaxins Sso1p and Sso2p belong to a family of related membrane proteins that function in vesicular transport. *EMBO J* 12, 4095–4104.
- Altschul SF, Gish W, Miller W, Myers EW, Lipman DJ (1990). Basic local alignment search tool. *J Mol Biol* 215, 403–410.
- Ashery U, Bielopolski N, Barak B, Yizhar O (2009). Friends and foes in synaptic transmission: the role of tomosyn in vesicle priming. *Trends Neurosci* 32, 275–282.
- Brennwald P, Kearns B, Champion K, Keränen S, Bankaitis V, Novick P (1994). Sec9 is a SNAP-25-like component of a yeast SNARE complex that may be the effector of Sec4 function in exocytosis. *Cell* 79, 245–258.
- Buvelot Frei S, Rahl PB, Nussbaum M, Briggs BJ, Calero M, Janeczko S, Regan AD, Chen CZ, Barral Y, Whittaker GR, Collins RN (2006). Bioinformatic and comparative localization of Rab proteins reveals functional insights into the uncharacterized GTPases Ypt10p and Ypt11p. *Mol Cell Biol* 26, 7299–7317.
- Comeau SR, Gatchell DW, Vajda S, Camacho CJ (2004). ClusPro: a fully automated algorithm for protein–protein docking. *Nucleic Acids Res* 32, W96–W99.
- De Lorenzo C, Mechler BM, Bryant PJ (1999). What is Drosophila telling us about cancer? *Cancer Metastasis Rev* 18, 295–311.
- Dey S, Pal A, Chakrabarti P, Janin J (2010). The subunit interfaces of weakly associated homodimeric proteins. *J Mol Biol* 398, 146–160.
- Eswar N, Webb B, Marti-Renom MA, Madhusudhan MS, Eramian D, Shen MY, Pieper U, Sali A (2006). Comparative protein structure modeling using MODELLER. *Curr Protoc Bioinformatics* Chapter 5, Unit 5.6.
- Fasshauer D, Jahn R (2007). Budding insights on cell polarity. *Nat Struct Mol Biol* 5, 360–362.
- Fujita Y, Shirataki H, Sakisaka T, Asakura T, Ohya T, Kotani H, Yokoyama S, Nishioka H, Matsuura Y, Mizoguchi A, *et al.* (1998). Tomosyn: a syntaxin-1-binding protein that forms a novel complex in the neurotransmitter release process. *Neuron* 20, 905–915.
- Gangar A, Rossi G, Andreeva A, Hales R, Brennwald P (2005). Structurally conserved interaction of Lgl family with SNAREs is critical to their cellular function. *Curr Biol* 15, 1136–1142.
- Grosshans BL, Andreeva A, Gangar A, Niessen S, Yates III JR, Brennwald P, Novick P (2006). The yeast lgl family member Sro7 is an effector of the secretory Rab GTPase Sec4p. *J Cell Biol* 172, 55–66.
- Guo W, Roth D, Walch-Solimena C, Novick P (1999). The exocyst is an effector for Sec4p, targeting secretory vesicles to sites of exocytosis. *EMBO J* 18, 1071–1080.
- Hattendorf DA, Andreeva A, Gangar A, Brennwald PJ, Weis WI (2007). Structure of the yeast polarity protein Sro7 reveals a SNARE regulatory mechanism. *Nature* 446, 567–571.
- Heider MR, Munson M (2012). Exorcising the exocyst complex. *Traffic* 13, 898–907.
- Higgins DG, Sharp PM (1988). CLUSTAL: a package for performing multiple sequence alignment on a microcomputer. *Gene* 73, 237–244.
- Hutterer A, Betschinger J, Petronczki M, Knoblich JA (2004). Sequential roles of Cdc42, Par-6, aPKC, and Lgl in the establishment of epithelial polarity during Drosophila embryogenesis. *Dev Cell* 6, 845–854.
- Jones JC, Jones AM, Temple BR, Dohlman HG (2012). Differences in intradomain and interdomain motion confer distinct activation properties to structurally similar G α proteins. *Proc Natl Acad Sci USA* 109, 7275–7279.
- Kagami M, Toh-e A, Matsui Y (1998). Sro7p, a *Saccharomyces cerevisiae* counterpart of the tumor suppressor l(2)gl protein, is related to myosins in function. *Genetics* 149, 1717–1727.
- Klopper TH, Kienle CN, Fasshauer D (2008). SNAREing the basis of multicellularity: consequences of protein family expansion during evolution. *Mol Biol Evol* 25, 2055–2068.
- Lazar T, Gotte M, Gallwitz D (1997). Vesicular transport: how many Ypt/Rab-GTPases make a eukaryotic cell? *Trends Biochem Sci* 22, 468–472.
- Lehman K, Rossi G, Adamo JE, Brennwald P (1999). Yeast homologues of tomosyn and lethal giant larvae function in exocytosis and are associated with the plasma membrane SNARE, Sec9. *J Cell Biol* 146, 125–140.

- Levin KB, Dym O, Albeck S, Magdassi S, Keeble AH, Kleanthous C, Tawfik DS (2009). Following evolutionary paths to protein-protein interactions with high affinity and selectivity. *Nat Struct Mol Biol* 16, 1049–1055.
- Lipatova Z, Hain AU, Nazarko VY, Segev N (2015). Ypt/Rab GTPases: principles learned from yeast. *Crit Rev Biochem Mol Bio* 23, 1–9.
- Moerschell RP, Das G, Sherman F (1991). Transformation of yeast directly with synthetic oligonucleotides. *Methods Enzymol* 194, 362–369.
- Protopopov V, Govindan B, Novick P, Gerst JE (1993). Homologs of the synaptobrevin/VAMP family of synaptic vesicle proteins function on the late secretory pathway in *S. cerevisiae*. *Cell* 74, 855–861.
- Rossi G, Watson K, Demonch M, Temple B, Brennwald P (2015). In vitro reconstitution of Rab GTPase-dependent vesicle clustering by the yeast lethal giant larvae/tomosyn homolog, Sro7. *J Biol Chem* 290, 612–624.
- Sakisaka T, Baba T, Tanaka S, Izumi G, Yasumi M, Takai Y (2004). Regulation of SNAREs by tomosyn and ROCK: implication in extension and retraction of neurites. *J Cell Biol* 166, 17–25.
- Salminen A, Novick PJ (1987). A ras-like protein is required for a post-Golgi event in yeast secretion. *Cell* 49, 527–538.
- Strand D, Jakobs R, Merdes G, Neumann B, Kalmes A, Heid HW, Husmann I, Mechler BM (1994). The *Drosophila* lethal(2)giant larvae tumor suppressor protein forms homo-oligomers and is associated with nonmuscle myosin II heavy chain. *J Cell Biol* 127, 1361–1373.
- Stroupe C, Brunger AT (2000). Crystal Structures of a Rab protein in its inactive and active conformations. *J Mol Biol* 304, 585–598.
- Thompson JD, Gibson TJ, Plewniak F, Jeanmougin F, Higgins DG (1997). The CLUSTAL_X windows interface: flexible strategies for multiple sequence alignment aided by quality analysis tools. *Nucleic Acids Res* 25, 4876–4882.
- Vasioukhin V (2006). Lethal giant puzzle of Lgl. *Dev Neurosci* 28, 13–24.
- Vetter JR, Wittinghoffer A (2001). The guanine nucleotide-binding switch in three dimensions. *Science* 294, 1299–1304.
- Wadskog I, Maldener C, Proksch A, Madeo F, Adler L (2004). Yeast lacking the SRO7/SOP1-encoded tumor suppressor homologue show increased susceptibility to apoptosis-like cell death on exposure to NaCl stress. *Mol Biol Cell* 15, 1436–1444.
- Walch-Solimena C, Collins RN, Novick PJ (1997). Sec2p mediates nucleotide exchange on Sec4p and is involved in polarized delivery of post-Golgi vesicles. *J Cell Biol* 137, 1495–1509.
- Wang T, Liu Y, Xu XH, Deng CY, Wu KY, Zhu J, Fu XQ, He M, Luo ZG (2011). Lgl1 activation of rab10 promotes axonal membrane trafficking underlying neuronal polarization. *Dev Cell* 21, 431–444.
- Williams AL, Bielopolski N, Meroz D, Lam AD, Passmore DR, Ben-Tal N, Ernst SA, Ashery U, Stuenkel EL (2011). Structural and functional analysis of tomosyn identifies domains important in exocytic regulation. *J Biol Chem* 286, 14542–14553.
- Zhang X, Wang P, Gangar A, Zhang J, Brennwald P, Terbush D, Guo W (2005). Lethal giant larvae proteins interact with the exocyst complex and are involved in polarized exocytosis. *J Cell Biol* 170, 273–283.